

Along-shore movement of groundwater and its effects on seawater-groundwater interactions in heterogeneous coastal aquifers

Xiaolong Geng¹, and Holly A. Michael^{1, 2*}

¹Department of Earth Sciences, University of Delaware, 225 Academy St., Newark, DE, 19716, USA

²Department of Civil and Environmental Engineering, University of Delaware, 102 Dupont Hall, Newark, DE, 19716, USA

*: Corresponding Author: Tel. +1 302-831-4197, Email: hmichael@udel.edu

Accepted Article

Abstract

Studies of coastal groundwater dynamics often assume two-dimensional (2D) flow and transport along a shore-perpendicular cross-section. We show that along-shore movement of groundwater may also be significant in heterogeneous coastal aquifers. Simulations of groundwater flow and salt transport incorporating different geologic structure show highly three-dimensional (3D) preferential flow paths. The along-shore movement of groundwater on average accounts for 40%-50% of the total flowpath length in both conduit-type (e.g., volcanic) heterogeneous aquifers and statistically equivalent (e.g., deltaic) systems generated with sequential indicator simulation (SIS). Our results identify a critical role of three-dimensionality in systems with connected high-permeability geological features. 3D conduit features connecting land and sea cause more terrestrial groundwater flow through inland boundary and intensify water exchange along the land-sea interface. Therefore, they increase the rate of SGD compared to equivalent homogeneous, SIS and corresponding 2D models. In contrast, in SIS-type systems, less-connected high-permeability features produce mixing zones and SGD nearer to shore, with comparable rates in 3D and 2D models. Onshore, 3D Heterogeneous cases have longer flowpaths and travel times from recharge to discharge compared to 2D cases, but offshore travel times are much lower, particularly for conduit-type models in which flow is highly preferential. Flowpath lengths and travel times are also highly variable in 3D relative to 2D for all heterogeneous simulations. The results have implications for water resources management, biogeochemical reactions within coastal aquifers, and subsequent chemical fluxes to the ocean.

Key Words

Heterogeneity; volcanic aquifers; lateral groundwater flow; conduits; submarine groundwater discharge; groundwater-seawater exchange

Key Points

- Geologic heterogeneity causes significant along-shore movement of groundwater in coastal heterogeneous aquifers
- Existence of along-shore groundwater flow in heterogeneous aquifers increases variability of travel length and time of terrestrial groundwater prior to discharge
- Connected, high-permeability features increase the rate of SGD compared to equivalent homogeneous, SIS and corresponding 2D models

Plain Language Summary

The findings of this study provide insight into the complex patterns of groundwater flow under the influence of geologic variability in coastal aquifers. In coastal regions, studies of solute transport processes mainly rely on an assumption of 2D groundwater flow and solute transport in the shore-perpendicular direction. Our results reveal that groundwater does not only flow toward the sea, it also can flow along-shore, especially in aquifers with features that connect the onshore and offshore. This affects exchange and mixing between fresh and saline groundwater, which can strongly impact delivery of contaminants and nutrients to sensitive nearshore marine ecosystems. Results highlight the importance of characterizing the geology of coastal aquifers and representing it in models of groundwater flow and contaminant transport.

1. Introduction

Groundwater has been recognized as one of the key factors affecting coastal marine ecological and biogeochemical processes [Johannes, 1980; Simmons Jr, 1992; Miller and Ullman, 2004; Santos et al., 2008; Kim et al., 2017]. Submarine groundwater discharge (SGD) provides a significant transport pathway for land-derived chemicals (e.g., nutrients, contaminants, and trace elements) to enter nearshore marine ecosystems [Burnett et al., 2003; Slomp and Van Cappellen, 2004; Defeo et al., 2009]. An elevated inland water table generally drives terrestrial groundwater to discharge from inland aquifers to the coastal ocean. In response to oceanic forcing (e.g., tides and waves) and the density difference between saltwater and freshwater, terrestrial groundwater undergoes significant mixing with saline groundwater prior to discharge [Boufadel, 2000; Horn, 2002; Michael et al., 2005; Robinson et al., 2007; Li et al., 2008; Xin et al., 2010; Geng et al., 2017]. The mixing zone between fresh and saline coastal groundwater, also referred to as the transition zone, has been recognized as an important reaction zone in nearshore aquifer, which has strong implications for chemical transformations [e.g., Moore, 1999; Charette and Sholkovitz, 2002; Beck et al., 2007; Santos et al., 2012; Kim et al., 2017; Kim et al., 2019b].

Over the past three decades, numerous studies have been conducted to investigate groundwater flow and associated mixing with seawater in coastal aquifers [Horn, 2002; 2006; Santos et al., 2012; Geng and Boufadel, 2017; Robinson et al., 2018]. Geologic heterogeneity has been identified as a critical factor affecting transport processes over many length scales, particularly for coastal aquifers where variable-density flow and transport occurs [Simmons et al., 2001]. Dagan and Zeitoun [1998] first adopted a sharp-interface approach to investigate effects of a layered one dimensional (1D) heterogeneity on seawater-freshwater interface in a confined aquifer. While the sharp-interface approach has been then widely used to investigate heterogeneity effects on coastal saltwater intrusion processes, this type of theoretical analysis assumes that the seawater and freshwater are separated by a sharp interface, and therefore, mixing dynamics cannot be assessed [Al-Bitar and Ababou, 2005; Chang and Yeh, 2010; Dokou

and Karatzas, 2012]. Numerical studies of geologic heterogeneity affecting groundwater-seawater mixing in coastal aquifers were first investigated by the classic benchmark problem for variable density flow, Henry problem [Henry, 1959; Held et al., 2005; Abarca, 2006]. Held et al. [2005] used homogenization theory to derive expressions for effective hydraulic conductivity and dispersivity in 2D isotropic and anisotropic heterogeneous permeability fields. Their numerical results showed that heterogeneity in permeability affects foremost the transient evolution of saltwater intrusion, whereas the steady-state saltwater distribution is less sensitive to spatially varying permeability and longitudinal dispersion. Abarca [2006] integrated natural heterogeneity into the Henry problem. They found that the shape of the interface and the saltwater flux strongly correlates to the distribution of the permeability in each geological realization. Michael et al. [2016] used lithologic data to develop geostatistical models that represent the architecture of coastal aquifers. Their simulation results of groundwater flow and salt transport through random geologic realizations indicate that heterogeneity produces spatially complex subsurface salinity distributions that extends tens of kilometers offshore. In highly heterogeneous coastal aquifers, in particular for fractured and karst systems, networks of high permeability geologic structures are also found to play an important role in nearshore groundwater flow and associated mixing with seawater [Ghasemizadeh et al., 2012; Sebben et al., 2015; Sebben and Werner, 2016; Xu et al., 2016; Montiel et al., 2018; Xu et al., 2018]. For instance, Sebben and Werner [2016] employed the discrete fracture network (DFN) approach to simulate solute transport through a 2-D permeable porous media containing a single, discrete preferential flow feature, elucidating considerable impacts of preferential flows on solute plume displacement and spreading.

While these studies show the importance of heterogeneity in 2D systems, studies on coastal groundwater flow and transport processes through 3D heterogeneous fields are rare, most likely due to the high computational cost of such simulations [Kerrou and Renard, 2010; Siena and Riva, 2018]. Kerrou and Renard [2010] conducted both 2D and 3D simulations to investigate heterogeneity effects on advective dispersive

seawater intrusion processes. They found that when the variance of the log hydraulic conductivity increases, the toe penetration reduces in 2D simulations, while it may increase or decrease in 3D simulations depending on the degree of heterogeneity and anisotropy. *Siena and Riva* [2018] conducted 3D groundwater simulations in a randomly heterogeneous aquifer. They found that the toe penetration and extent of the mixing zone in heterogeneous systems tend to be, respectively, smaller and larger compared to their equivalent homogeneous systems. Experimental studies have also been conducted to assess how the complexity of heterogeneity influences nearshore salinity distributions in coastal aquifers [*Lu et al.*, 2013; *Nofal et al.*, 2015; *Montiel et al.*, 2018]. *Lu et al.* [2013] conducted laboratory experiments, complemented with numerical simulations, and identified significant impacts of aquifer stratification on the spatial extent of the freshwater-seawater mixing zone. *Houben et al.* [2018] conducted physical experiments and numerical modeling to investigate the influence of geological heterogeneity on coastal groundwater flow. The study revealed that fringing reefs, acting as low-permeability caprocks, led to a bimodal regime of freshwater discharge, with discharge at the beach face and through deeper submarine springs. In addition, vertical dykes on volcanic islands, acting as impermeable vertical flow barriers, led to impoundment of fresh groundwater and compartmentalization of the aquifer, which significantly altered the shape of the freshwater-seawater interface. *Montiel et al.* [2018] revealed significant spatial variability of groundwater discharge via submarine springs due to extensive development of the spring conduits in highly heterogeneous karst aquifer systems.

While considerable research effort has been made to characterize groundwater flow and freshwater-saltwater mixing in coastal aquifers, only a few studies have investigated along-shore groundwater flow (i.e., movement of groundwater in along shore direction) and its influence on transport processes. *Abarca et al.* [2007] revealed that along-shore groundwater flow could be significant when nearshore aquifers exhibit a large variability in the topography. Through numerical simulations, *Knight et al.* [2021] demonstrated that alongshore head gradients generated significant amount of

alongshore freshwater circulation in coastal semi-confined aquifer systems. In heterogeneous aquifers, three-dimensional geological features may also cause significant along-shore movement of groundwater through preferential pathways oblique to the large-scale hydraulic gradient, which could significantly alter nearshore salinity distributions [*Siena and Riva, 2018*]. Networks of high-permeability geologic structures can also be a critical factor, causing along-shore groundwater flow. For instance, volcanic aquifers are formed by laterally spreading lava flows that effused from fissures and vents [*Oki et al., 1999; El-Kadi and Moncur, 2006*], potentially resulting in continuous, connected high-permeability conduit structures formed by voids and fractures along the direction of lava flows [*Helm-Clark et al., 2004; Gingerich, 2008*]. The unique geologic heterogeneity and associated preferential flow could result in highly three-dimensional groundwater flow in volcanic aquifers. Therefore, along-shore movement of groundwater may also play an important role in altering groundwater flow paths, salinity distributions, and rates and patterns of SGD in highly heterogeneous coastal aquifers. Despite its potential importance, the three-dimensional nature of heterogeneous coastal aquifers is rarely assessed, as the computational burden of simulating variable-density flow and transport is high.

The goal of this study is to quantify along-shore groundwater movement and its associated influences on patterns of salinity and SGD in heterogeneous coastal aquifers. We investigated along-shore groundwater movement in different types of heterogeneous fields by adopting a hybrid modeling method to generate representations of volcanic, or conduit-type, aquifer structures and statistically equivalent geological realizations with sequential indicator simulation more typical of sedimentary systems such as deltas. We conducted groundwater flow and salt transport simulations to identify the patterns of groundwater flow and salt transport, and compared them to the results derived from the simulations conducted along corresponding 2D heterogeneous across-shore transects and equivalent homogeneous systems. The results highlight the influence of geologic heterogeneity on three-dimensional along-shore groundwater movement, freshwater-saltwater mixing, and SGD in coastal aquifers.

2. Methods

Models of conduit-type aquifer heterogeneity were developed using a hybrid modeling scheme based on a volcanic system. A process-based model, simulating volcanic eruptions and associated lava emplacement, was first adopted to obtain geometrical parameters. A geostatistical surface-based model that incorporated the geometric parameters was then used to simulate a series of depositional events and individual lava paths to create a volcanic aquifer [Koneshloo *et al.*, 2018]. The statistics used for the simulations were derived from data from the Big Island of Hawai'i. Six three-dimensional volcanic heterogeneous fields, each comprised of 15,000 volcanic eruption events, were simulated on a $10\text{ m} \times 10\text{ m} \times 2\text{ m}$ grid (referred to as *conduit* field); the models are the same as those in Kreyms *et al.* [2020]. The simulations considered six facies: aa, pahoehoe, clinker, tube, transitional lava, and ash, with proportions about $\sim 74.1\%$, $\sim 10.2\%$, $\sim 5.6\%$, $\sim 6.5\%$, $\sim 3.4\%$, and $\sim 0.2\%$, respectively. Representative values of hydraulic conductivity (K) assigned to each of the six facies were: 10^{-7} m/s , 10^{-5} m/s , 10^{-3} m/s , 10^{-1} m/s , 10^{-6} m/s and 10^{-9} m/s , respectively. The facies percentages and corresponding K values adopted in this paper are consistent with values found in literature [Hunt *et al.*, 1988; Miller *et al.*, 1997; Anderson *et al.*, 1999; Ducci, 2010], approximating proportions observed in a core through Mauna Loa and Mauna Kea deposits $\sim 40\text{ km}$ from a vent [Garcia *et al.*, 2007], but with higher aa and lower pahoehoe proportions to represent a Hualalai-type system at a distance of $\sim 12\text{ km}$ from a vent [Wentworth and Macdonald, 1953; Rowland and Walker, 1990]. Note that the geologic structures are different among these six fields due to random seeds in the model, but statistically equivalent due to the same statistical input.

A 3D domain, representing the saturated portion of the nearshore aquifer, was extracted from each heterogeneous K -field and used for simulating groundwater flow and salt transport processes at a similar distance from the vent as the Kahaluu Beach Park is from the Hualalai vent (Figure 1). The size of the domain was 1000 m in the across-

shore direction (X -axis), 300 m in the along-shore direction (Y -axis). The vertical size of the domain (Z -axis) was 100 m at the onshore boundary and gradually decreased from 100 m to 10 m at the offshore boundary, which is consistent with nearshore Hawai'i bathymetry data from NOAA's National Center for Environmental Information (NCEI) (<https://maps.ngdc.noaa.gov/viewers/bathymetry>).

Statistically equivalent geologic realizations were generated by the geostatistical method of sequential indicator simulation using SGeMS software [Remy *et al.*, 2009], referred to as *SIS fields*. Each SIS field was simulated based on the histogram and variogram model derived from the corresponding conduit field (Figures S1 and S2) [Michael *et al.*, 2016; Geng and Michael, 2020]. Equivalent homogeneous fields were also used for comparison. Effective K values for the equivalent homogeneous models were determined by simulating horizontal and vertical flow through each conduit K -field across a specific head gradient using MODFLOW [Harbaugh, 2005]. Resulting total fluid fluxes across horizontal and vertical boundaries were used with Darcy's Law to calculate anisotropic effective K values. In such case, an equivalent total flux will be derived from conduit and corresponding homogeneous fields when a specific head gradient is applied.

Three-dimensional (3D) simulations of variable-density groundwater flow and salt transport were conducted through each K -field using SEAWAT v4.0 [Langevin *et al.*, 2008]. The 3D domain was discretized using a $100 \times 30 \times 50$ ($X \times Y \times Z$) grid, which is the same as the grid used in the geostatistical modeling. Two-dimensional (2D) simulations (30 2D across-shore transects for each 3D case), neglecting along-shore groundwater flow, were also conducted through each across-shore heterogeneous transect for comparison. In the simulations, a constant head of 2.5 m was assigned to the landward vertical boundary. The groundwater head of 2.5 m is within the range of the groundwater table observations around the Big Island of Hawaii that varies from 0.5 m to 4.5 m above the mean sea level (MSL) at an onshore distance similar to the model setup (<https://waterdata.usgs.gov/nwis>). The ocean was represented as a

specified hydraulic head boundary along the offshore model top and offshore vertical boundary. The salinity specified on the landward and seaward boundaries was 0 g/l and 35 g/l, respectively. Zero flux for both groundwater flow and salt transport was assigned to the rest of the boundaries. Values of longitudinal, horizontal transverse, and vertical transverse dispersivity were 4 m, 0.4 m, and 0.04 m, respectively. The molecular diffusion coefficient was 10^{-9} m²/s. The simulations were run for 1000 years until hydraulic heads and concentrations reached steady state, which is identified by the discrepancy of hydraulic head and salinity distribution between two time steps consistently less than 0.1%.

Particle tracking was conducted to quantify groundwater flow patterns and associated transit times using the steady-state velocity fields derived from the SEAWAT simulations. The neutrally buoyant particles were released at two along-shore locations (Y =140 and 200 m) and at two across-shore locations (onshore and offshore). The onshore particles were released at 10 m depth interval along the vertical inland boundary, spanning from Z = 0 to -100 m, and forward tracked. Both forward and backward particle tracking schemes were used for offshore released particles to assess particle transit time at recharge points and particle trajectory at discharge points among the cases, respectively. For forward particle tracking, offshore particles were released along the sea floor boundary from X =550 m to 700 m for all the cases. For backward particle tracking, offshore particles were released at 10 m intervals from X = 500 to 750 m for 3D conduit cases. The discharge zone for 2D and 3D SIS and homogeneous cases and 2D conduit cases only occurred near the shoreline; therefore, for those cases, offshore particles were released with a higher resolution of 0.1 m from X = 500 to 600 m. The movement of each particle in a certain direction with respect to its overall travel length, M_s , was quantified, expressed as:

$$M_s = \frac{\sum_{i=1}^{N_T} v_{si} \cdot \Delta t}{\sum_{i=1}^{N_T} \sqrt{v_{xi}^2 + v_{yi}^2 + v_{zi}^2} \cdot \Delta t} \times 100\% . \quad (1)$$

Where $s = x, y,$ or z , representing across-shore, along-shore and vertical directions,

respectively; Δt is time step; $N_T \cdot \Delta t$ represents the total transit time of the particles in the aquifer; $v_{si} \cdot \Delta t$ represents the replacement of particles in s -direction at the i th time step.

The size and offshore extent of the mixing zone along each simulated across-shore transect was quantified for 3D and 2D as the area with salinity between 10% and 90% seawater, and total fresh and saline SGD was calculated. The location of the centroid of the mixing zone was also determined based on the mass distribution. To compute the mixing zone volume for 2D cases, along-shore thickness was assumed to be 10 m so that the total aquifer volume was the same for 3D and corresponding 2D cases.

3. Results

The 3D simulations of variable-density groundwater flow and salt transport consistently show different salinity distributions compared to those of corresponding 2D models for both conduit and SIS cases (Figures 2 and 3). In particular, for conduit cases, 3D simulations produced a more seaward mixing zone between fresh and saline groundwater. This is mostly likely due to 3D preferential flows produced in the 3D simulations, creating additional flow paths (i.e., 3D flow structure) that drive terrestrial fresh groundwater to discharge and mix with seawater farther offshore. In both conduit and SIS models, there is a clear difference in salinity distributions between the 2D and 3D simulations (Figure 3). Note that there is no difference between 2D and 3D simulations for homogeneous cases due to a homogeneous K field and zero hydraulic gradient between the two along-shore boundaries (Figure S3).

The shape and size of the mixing zone was also affected by the 3D flowpaths. For conduit cases, 2D models have similar mixing zones, whereas for SIS cases, 3D models have larger mixing zones (Figure 4). For conduit cases, the slightly larger mixing zone on average in 2D models are most likely due to lower connectivity of high-permeability geologic structures, resulting in less freshwater recharge, landward intrusion of

saltwater, and more mixing with fresh groundwater. The 3D conduits conduct much of the freshwater directly offshore, thereby enhancing offshore contact between fresh and saline groundwater. Thus, for conduit cases, the mixing zone is larger offshore but smaller onshore, producing comparable mixing volumes but quite different salinity distributions (Figure S4). In contrast, for SIS cases, high-permeability geologic features exhibit relatively lower connectivity. Therefore, with comparable landward extent of the mixing zone, 3D geological structures enhance groundwater mixing, resulting in larger mixing zones for 3D SIS models compared to 2D SIS models. Compared to homogeneous models, all heterogeneous models demonstrate larger mixing zones, indicating the significant role of geologic heterogeneity in enhancing nearshore groundwater-seawater mixing in coastal aquifers that are not dominated by preferential flow conduits. This reasoning is consistent with the results of the location of the mixing zone centroid, showing that its average location in 2D and 3D models was 497 m and 644 m, 386 m and 386 m, and 497 m and 478 m for conduit, homogeneous, and SIS cases, respectively (Figure 5).

The patterns of groundwater flow are shown using particle tracking. Examples of simulated particle trajectories for conduit cases show that the inland-released, forward-tracked particles migrated seaward along several preferential paths that converged when they approached the shoreline (Figures 6a and 6b). In contrast, the offshore-released, backward-tracked particles flowed landward along offshore density-driven circulation flow paths which were greatly perturbed by aquifer heterogeneity (Figures 6a and 6c) compared to the smooth and shore-perpendicular paths of the equivalent homogeneous aquifer (Figures 6d-6f). Significant along-shore movement for both onshore and offshore particles is evident in the conduit case. For the inland-released particles, the offshore preferential discharge points laterally shift up to ~150 m with respect to their onshore release locations (e.g., shifted from $y=150$ to $y \sim 300$ m). The particle trajectories for SIS cases also demonstrate significant along-shore movement (Figures 6g-6i). However, compared to corresponding conduit cases, in which nearly all of the particles converged into one preferential flowpath, the onshore-released

particles in the SIS cases followed more independent flow paths (Figure S3). In addition, the discharge locations of the offshore-released particles for SIS cases mostly occurred near the shoreline, and farther offshore circulation flow paths were not dominant.

The along-shore movement of groundwater and associated impacts on flow patterns in heterogeneous models were also identified by comparing 3D to corresponding 2D models. Figure 7 shows the travel distance of particles in each direction (D_s), for all heterogeneous and homogeneous realizations. The average along-shore movement of onshore and offshore particles was 353 m and 168 m for conduit cases, accounting for 42% and 47% of the total travel length for 3D and 2D simulations, respectively. The along-shore movement was substantial in 3D SIS cases as well, with average distances of 375 m and 213 m, accounting for 45% and 50% of the total travel length for onshore and offshore particles for 3D and 2D simulations, respectively.

Along-shore groundwater flow also significantly affects total travel length and travel time of the inland-released particles. The travel lengths were longer for 3D heterogeneous models than for the corresponding 2D models and homogeneous cases (Figure 8a). This is expected because heterogeneity-induced 3D flow, particularly along-shore groundwater flow, elongated the flowpaths of the particles originating from inland. Compared to corresponding 2D models, the travel lengths of the inland particles for 3D heterogeneous models were also more variable, the mean \pm standard deviation equal to 850 m \pm 120 m and 820 m \pm 100 m for conduit and SIS cases, respectively, compared to 560 m \pm 20 m and 580 m \pm 40 m for the corresponding 2D models. This indicates that the 3D heterogeneous fields greatly enhanced the complexity of flow paths in both types of aquifer systems. In contrast, travel lengths are identical for 3D and 2D homogeneous models due to the absence of along-shore groundwater movement. The travel times of inland-released particles were also more variable in 3D fields relative to 2D (Figure 8b), particularly for conduit models. The median \pm standard deviation of travel time for 3D conduit models was 3467 \pm 10,000 years, compared to 4000 \pm 2000 years for corresponding 2D models. In SIS cases, travel times were

somewhat less variable in 3D, with median \pm standard deviations of 1100 ± 3000 years for 3D and 2200 ± 2000 years for 2D models. The travel time of particles for equivalent homogeneous cases was much shorter on average, and with a smaller median \pm standard deviation of 53 ± 54 years.

The travel times of offshore-release particles are also affected by along-shore groundwater flow. The travel times of particles released in offshore recharge locations spanning from $x = 550$ m to 700 m at 10 m intervals along $Y = 140$ m and 200 m are shown in Figures 9 and S5. Note that forward particle tracking was adopted, and therefore, zero travel time implies groundwater discharge points. The travel times for 3D conduit models are slightly shorter and more variable compared to corresponding 2D models. The recharge gap between $x = 630$ m and 670 m for the 3D conduit case represents groundwater discharge occurring farther offshore. In contrast, for equivalent homogeneous cases, the recharge points started to appear at 70 m offshore, and associated travel times tended to increase with distance offshore. Similarly, the SIS cases show nearshore discharge and relatively long travel times with distance offshore. Interestingly, although travel distances tend to be much greater for 3D vs 2D models for both onshore and offshore flow, the travel times do not always follow that pattern. We suggest that this is because connectedness through high-K sediments increases in 3D, whereas more water may be forced to flow through low-K sediments in 2D models.

The difference in connectivity among 2D and 3D models also explains differences in SGD and its variability. In many cases, fresh SGD was orders of magnitude greater in 3D models compared to 2D, particularly for conduit cases (Figure S6). This is likely due to 3D connected high-K features (i.e., higher effective K, shown in Figure S7), resulting in more freshwater flux through the constant head boundary on the landside. The difference in connectivity from 2D to 3D is greater for conduit cases than for SIS cases because the conduits do not follow a cross-shore transect. Fresh SGD along transects was also highly variable, varying from 10^{-5} m/d to 5.8 m/d and from 10^{-4} m/d to 0.5 m/d for 3D conduit and SIS models, respectively, compared to a narrow range

around 10^{-3} m/d for both sets of 2D models, and from $\sim 10^{-2}$ m/d to 0.3 m/d for homogeneous cases. In contrast, saline SGD was elevated for 3D conduit cases with respect to 2D, but not for SIS cases. Conduit cases also had greater variability in saline SGD in 3D, ranging from $\sim 10^{-4}$ m/d to 51 m/d, compared to homogeneous cases, which ranged from $\sim 10^{-1}$ m/d to 0.45 m/d (Figure 10a). For SIS cases, saline SGD was more comparable in 3D and 2D models, ranging from $\sim 10^{-4}$ m/d to 27 m/d and from $\sim 10^{-4}$ m/d to 12.7 m/d, respectively (Figure 10b).

4. Discussion

This study highlights the importance of geological heterogeneity and 3D flow in coastal aquifers, with implications for groundwater resource management. Assessment of nearshore groundwater resource sustainability relies on the effective delineation of nearshore salinity structure [Gibert *et al.*, 1994; Huyakorn *et al.*, 1996; Goswami and Clement, 2007; Abd-Elhamid and Javadi, 2011; Chang and Clement, 2012; Zhou *et al.*, 2012]. Gingerich and Voss [2005] conducted groundwater simulations for Pearl Harbor aquifer at southern Oahu, Hawaii, where the aquifer system was delineated by a basalt formation overlain by caprock. Their simulations revealed that the 3D model allowed simulation of localized saltwater intrusion when inland freshwater pumping occurred. Our simulation results show that geologic heterogeneity, in particular the existence of continuous, high-permeability features such as those in volcanic aquifers, creates 3D distributed salinity structures in nearshore aquifers. Compared to 3D models, 2D models neglecting along-shore movement of groundwater predict very different salinity distributions, indicating that 2D groundwater modeling or 2D monitoring might not be sufficient to characterize vulnerability and sustainability of coastal freshwater resources. In particular, as high-permeability conduits cause comparable along-shore flow to that in the across-shore direction, nearshore freshwater abstraction could create substantial uncertainty in both the volume of fresh groundwater being salinized and location of saltwater intrusion. 3D simulations produce significant along-shore bypass along preferential flows in volcanic aquifers (Figure S8a). As inland head drops (e.g., due to freshwater pumping), hydraulic gradients could be potentially reversed, resulting in

more landward saltwater intrusion through these 3D preferential pathways [e.g., *Geng and Michael, 2020*]. In comparison, the preferential flow paths predicted from 2D simulations neglect along-shore groundwater bypasses (e.g., Figure S8b), and therefore might not be able to capture along-shore uncertainty of saltwater intrusion in volcanic coastal aquifer systems. Our simulations indicate underestimation of preferential flows from 2D model in comparison to 3D models. As shown in Figure 11c, the volume of preferential flows predicted from the 3D models is almost two times larger than the volume predicted from the 2D models. Note that the preferential flow is defined as velocity magnitude over 5 orders of magnitude larger than the minimum velocity. Our simulations show consistent higher seaward pressure head (depth-averaged) for 3D models in comparison to 2D models (Figure S9). This is as expected because 3D connected conduits facilitate pressure transmission that emanates from inland. Such results indicate that 2D models may overestimate the inland extent of saline groundwater at steady-state in coastal volcanic aquifers compared to 3D models. In order to produce similar landward extent of saltwater intrusion to 3D models, hydraulic conductivity may need to be elevated in 2D models. However, depth-averaged pressure head predicted from 3D models also shows some localized jumps (e.g., Figure S9b, across sections 3 and 6), which are likely due to high permeability features surrounding low permeability features. This is unlikely to be produced by 2D models as along-shore connections are neglected.

Our findings also have strong implications on monitoring and investigation of SGD. The significant lateral movement of groundwater revealed in this analysis increases spatial variability of SGD in heterogeneous aquifers. The assumption of shore-perpendicular flow may be incorrect in field studies seeking to link onshore measurements to offshore discharge along a flowpath. Thus, an appropriate field design, taking into account geologic heterogeneity, would be essential for a comprehensive assessment of SGD in coastal aquifers. For example, a large number of seepage meter measurements, spanning in both along-shore and across-shore directions, may be required in heterogeneous systems in order to accurately characterize spatial variability

in SGD. In addition, geophysical techniques (e.g., measuring electrical conductivity, acoustic impedance, or temperature) could be an efficient tool to identify relatively large-scale salinity distributions and locations of fresh SGD [*Taniguchi et al.*, 2019; *Geng et al.*, 2021; *Moosdorf et al.*, 2021].

Our study demonstrates the importance of using 3D models to investigate groundwater mixing dynamics in highly heterogeneous aquifer systems. In most studies of freshwater-saltwater mixing dynamics in heterogeneous coastal aquifers, only shore-perpendicular cross-sections are considered [*Al-Bitar and Ababou*, 2005; *Yang et al.*, 2015; *Rathore et al.*, 2018; *Geng et al.*, 2020b; *Heiss et al.*, 2020]. Our simulation results demonstrate distinct salinity distributions produced from 3D and 2D shore-perpendicular models for both conduit and SIS cases. It indicates taking into account along-shore movement of groundwater flow is of importance to evaluate spatial patterns of nearshore groundwater-seawater mixing in coastal heterogeneous aquifer. The nature of 3D flow is also different in aquifers with connected high-K features compared to heterogeneous aquifers with less discrete features. 3D networks of high-permeability geologic features and associated groundwater flow likely produce greatly variable spatial extents of freshwater-seawater mixing zone in along-shore direction of coastal aquifers.

Although our 3D conduit models provide more realistic simulations to evaluate the influence of connected geologic features on coastal groundwater flow and transport processes than homogeneous or 2D models, many simplifying assumptions were made. For example, the current study neglects transient hydraulic boundaries such as seasonal oscillations of inland groundwater table and oceanic forcing (e.g., waves and tides), as well as longer timescale sea-level change, which could be relevant given the long time required for the simulations to reach steady state. While the primary conclusions of this work would not change for transient systems, heterogeneity affects response to transient forcing [i.e., *Geng et al.*, 2020a; *Geng and Michael*, 2020; *Geng et al.*, 2020b], and this should be considered in future work.

The simulation results also highlight the important implications of heterogeneity on nearshore pollution and geochemical reactions. On one hand, the highly variable three-dimensional flowpaths could lead to spreading of inland-derived pollutants and difficulty in remediating contamination such as oil spills [Neupauer *et al.*, 2014; Geng *et al.*, 2016; Lester *et al.*, 2016; Boufadel *et al.*, 2019]. In addition, the 3D flow paths increase uncertainty of when and where the main pollutants discharge from nearshore aquifers to the ocean. On the other hand, the tortuosity, mixing, and sometimes long travel times can reduce effects on nearshore marine waters of pollutants that attenuate in aquifers. For example, studies show that both longer freshwater flowpaths [e.g., Gonnee and Charette, 2014; Sawyer *et al.*, 2014], and greater mixing [e.g., Kim *et al.*, 2019a; Heiss *et al.*, 2020] result in greater denitrification, thereby reducing the bioavailable nitrogen load that leads to eutrophication in coastal waters.

5. Conclusion

Simulations of groundwater flow and salt transport show significant along-shore movement of groundwater in highly heterogeneous coastal aquifers, which leads to highly 3-D groundwater flow and solute transport processes. The existence of along-shore groundwater flow increases the variability of travel length and travel time of terrestrial groundwater prior to discharge into the ocean. Simulations of groundwater flow through 3D heterogeneous structures show a comparable length of flowpaths in along-shore direction to that in across-shore direction for both conduit and SIS cases. The particle tracking results show such along-shore movement results in longer travel lengths with larger variations for the particles originating from inland for 3D heterogeneous models than for the corresponding 2D models and homogeneous cases. It also shows that simulations with 3D conduit features produced travel times of flow prior to discharge almost 2 times higher than that simulated from corresponding 2D models. However, greater travel lengths in 3D vs 2D simulations did not always correspond to a similar reduction in travel time, in fact, for offshore-released particles, 2D travel times on average were in several cases greater than those in 3D, indicating

that three-dimensionality may increase connectedness thereby reducing the amount of flow through low-permeability sediments.

Our results also identify an important role of connected high-permeability features in terrestrial groundwater flow patterns and associated interactions with offshore seawater. The 3-D networks of high-permeability conduits induce more highly preferential flow, which drives terrestrial fresh groundwater to migrate farther offshore. It consequently elevated the magnitude of saline and fresh SGD, compared to corresponding 2D cases and homogenous cases. In addition, 3D models and corresponding 2D models predict distinct salinity distributions for both conduit and SIS cases. In particular, 3D conduit models predict greater variability of spatial extents of freshwater-seawater mixing zone. This study highlights the importance of the geometry of geologic features and 3D flow in understanding coastal groundwater flow and solute transport processes in highly heterogeneous aquifers. The findings have important implications for water resources, biogeochemical conditions, and consequent nutrient cycling and contaminant transport from onshore to offshore, highlighting the necessity of taking into account three-dimensional geologic heterogeneity and preferential flow in investigating coastal transport and reaction processes in highly heterogeneous aquifers.

Acknowledgements This work was funded by the U.S. National Science Foundation EAR1151733 to H.M. Modeling files are available from the CUAHSI HydroShare database (Geng & Michael, 2021, <https://doi.org/10.4211/hs.1300844ad3c647f3ab9c6c221f8747ae>).

Captions:

Figure 1 Model setup. Boundary conditions implemented in the three-dimensional simulations of groundwater flow and salt transport using SEAWAT v4.0. The simulations were run to steady state for hydraulic heads and concentrations. The neutrally buoyant particles were released at two alongshore locations ($Y=14$ and 20 m) and at two across-shore locations (onshore and offshore). The onshore particles were released at 10 m depth interval along the vertical inland boundary, spanning from $Z = 0$ to -100 m. The offshore particles were released along the sea floor boundary from X

=550 m to 700 m.

Figure 2 Example of heterogeneous K fields for (a) conduit and (b) SIS cases, respectively. The $\log(K/K_{\min})$ values of 0, 2, 3, 4, 6, 8 denote the heterogeneous facies of ash, aa, transitional lava, pahoehoe, clinker and lava tube, respectively.

Figure 3 Example of simulated 3D (a, c) and 2D (b, d) steady-state salinity distributions for (a, b) conduit and (c, d) SIS cases, respectively. White lines in a and b show locations of transition zone for corresponding equivalent homogeneous cases. Gray conduits in a and c show preferential flow zones with velocity 8 orders of magnitude higher than minimum velocity simulated in each heterogeneous field.

Figure 4 Comparison of mixing zone volume for the simulated cases. Note that 2D and 3D Homogeneous cases are identical. Top and bottom of the rectangles represent the 25th and 75th percentiles of the data set. Solid line and cube indicate median and mean values, respectively. Whiskers indicate maximum and minimum values. Six geologic realizations were considered for conduit, equivalent homogeneous, and SIS cases.

Figure 5 Comparison of mixing zone centroid between 3D and 2D simulations for conduit, equivalent homogeneous, and SIS cases. The distance (in meter) shown in horizontal and vertical axes represents the mixing zone centroid of across-shore slices simulated by 2D and 3D models, respectively, for conduit, equivalent homogeneous, and SIS cases.

Figure 6 Examples of 3D trajectory of particles released from inland (left, top view) and offshore (right, top view) for (a-c) conduit, (d-f) equivalent homogeneous, and (g-i) SIS cases, respectively. Top view of the trajectories is to highlight lateral movement of particle flowpaths. Different particle trajectories are marked with different colors. The start and end locations of particle flow paths are marked with square and circle symbols, respectively; dashed line denotes shoreline location. Backward particle tracking scheme was implemented to trace trajectory of offshore particles, and thus particles released at recharge locations could not be traced. These recharge locations are marked in black for conduit cases; for equivalent homogeneous and SIS cases, offshore particles released within the groundwater discharge zone only occurred between $X = 500$ m and 550 m, and were marked with a black outline.

Figure 7 Travel distance in across-shore, along-shore, and vertical directions for particles released from (a) inland and (b) the seawater-groundwater recirculation zone, respectively, for all heterogeneous realizations. The lateral movement of groundwater (i.e., alongshore movement) was zero by definition in 2D cases. Bar, box, and line display the full range of variation (from min to max), the likely range of variation (i.e., from 25th percentile to 75th percentile), and the mean value, respectively.

Figure 8 Comparison of (a) travel length and (b) travel time of particles released from

inland between 2D and 3D conduit, equivalent homogeneous, and SIS cases. The particle travel length is calculated based on Eq. (1). The cross symbols marked with red and purple color represent the median travel time for conduit and SIS cases, respectively.

Figure 9 Examples of spatial distribution of travel time for particles released offshore, from the seawater-groundwater recirculation zone for (a) 3D conduit case, (b) 2D conduit case, (c) 3D homogeneous case, (d) 2D homogeneous case, (e) 3D SIS case, and (f) 2D SIS case. The particles were released in offshore recharge locations from $x = 550$ m to 700 m along $Y = 140$ m. Forward particle tracking was implemented to quantify travel time of particles released along the offshore major recharge zone with 10 m intervals.

Figure 10 Comparison of saline SGD (m/d) between 2D and 3D simulations for (a) conduit and equivalent homogeneous and (b) SIS cases.

References

- RELAP5/MOD3 Code Manual Volume I: Code Structure, System, Models, and Solution Methods. RELAP 5 Code Development Team. NUREG/CR-5535. INEL-95/0174 Volume I, edited, Idaho National Engineering Laboratory.
- Abarca, E. (2006), *Seawater intrusion in complex geological environments*, Universitat Politècnica de Catalunya.
- Abarca, E., J. Carrera, X. Sánchez-Vila, and C. I. Voss (2007), Quasi-horizontal circulation cells in 3D seawater intrusion, *Journal of Hydrology*, 339(3-4), 118-129.
- Abd-Elhamid, H., and A. Javadi (2011), A density-dependant finite element model for analysis of saltwater intrusion in coastal aquifers, *Journal of Hydrology*, 401(3-4), 259-271.
- Al-Bitar, A., and R. Ababou (2005), Random field approach to seawater intrusion in heterogeneous coastal aquifers: unconditional simulations and statistical analysis, in *Geostatistics for environmental applications*, edited, pp. 233-248, Springer.
- Anderson, S., M. A. Kuntz, and L. C. Davis (1999), Geologic controls of hydraulic conductivity in the Snake River Plain aquifer at and near the Idaho National Engineering and Environmental Laboratory, *IdahoRep.*, US Geological Survey, Idaho Falls, ID (US).
- Beck, A. J., Y. Tsukamoto, A. Tovar-Sanchez, M. Huerta-Diaz, H. J. Bokuniewicz, and S. A. Sanudo-Wilhelmy (2007), Importance of geochemical transformations in determining submarine groundwater discharge-derived trace metal and nutrient fluxes, *Applied Geochemistry*, 22(2), 477-490.
- Boufadel, M., X. Geng, C. An, E. Owens, Z. Chen, K. Lee, E. Taylor, and R. C. Prince (2019), A review on the factors affecting the deposition, retention, and biodegradation of oil stranded on beaches and guidelines for designing laboratory experiments, *Current Pollution Reports*, 5(4), 407-423.
- Boufadel, M. C. (2000), A mechanistic study of nonlinear solute transport in a groundwater-surface water system under steady state and transient hydraulic conditions, *Water Resources Research*, 36(9), 2549-2565.
- Burnett, W. C., H. Bokuniewicz, M. Huettel, W. S. Moore, and M. Taniguchi (2003), Groundwater and pore water inputs to the coastal zone, *Biogeochemistry*, 66(1-2), 3-33.
- Chang, C.-M., and H.-D. Yeh (2010), Spectral approach to seawater intrusion in heterogeneous coastal

- aquifers, *Hydrology and Earth System Sciences*, 14(5), 719-727.
- Chang, S. W., and T. P. Clement (2012), Experimental and numerical investigation of saltwater intrusion dynamics in flux - controlled groundwater systems, *Water Resources Research*, 48(9).
- Charette, M. A., and E. R. Sholkovitz (2002), Oxidative precipitation of groundwater - derived ferrous iron in the subterranean estuary of a coastal bay, *Geophysical research letters*, 29(10).
- Dagan, G., and D. G. Zeitoun (1998), Seawater-freshwater interface in a stratified aquifer of random permeability distribution, *Journal of Contaminant Hydrology*, 29(3), 185-203.
- Defeo, O., A. McLachlan, D. S. Schoeman, T. A. Schlacher, J. Dugan, A. Jones, M. Lastra, and F. Scapini (2009), Threats to sandy beach ecosystems: a review, *Estuarine, Coastal and Shelf Science*, 81(1), 1-12.
- Dokou, Z., and G. P. Karatzas (2012), Saltwater intrusion estimation in a karstified coastal system using density-dependent modelling and comparison with the sharp-interface approach, *Hydrological Sciences Journal*, 57(5), 985-999.
- Ducci, D. (2010), Aquifer vulnerability assessment methods: the non-independence of parameters problem, *Journal of Water Resource and Protection*, 2(04), 298.
- El-Kadi, A. I., and J. E. Moncur (2006), The history of groundwater management and research in Hawaii, paper presented at 2006 Jeju-Hawaii Water Forum, Proceedings, Jeju, Korea, July 21-22.
- Garcia, M. O., E. H. Haskins, E. M. Stolper, and M. Baker (2007), Stratigraphy of the Hawai 'i Scientific Drilling Project core (HSDP2): Anatomy of a Hawaiian shield volcano, *Geochemistry, Geophysics, Geosystems*, 8(2).
- Geng, X., and M. C. Boufadel (2017), The influence of evaporation and rainfall on supratidal groundwater dynamics and salinity structure in a sandy beach, *Water Resources Research*, 53(7), 6218-6238.
- Geng, X., J. W. Heiss, H. A. Michael, and M. C. Boufadel (2017), Subsurface flow and moisture dynamics in response to swash motions: Effects of beach hydraulic conductivity and capillarity, *Water Resources Research*, 53(12), 10317-10335.
- Geng, X., J. W. Heiss, H. A. Michael, M. C. Boufadel, and K. Lee (2020a), Groundwater flow and moisture dynamics in the swash zone: effects of heterogeneous hydraulic conductivity and capillarity, *Water Resources Research*, 56(11), e2020WR028401, doi:10.1029/2020WR028401.
- Geng, X., J. W. Heiss, H. A. Michael, H. Li, B. Raubenheimer, and M. C. Boufadel (2021), Geochemical fluxes in sandy beach aquifers: Modulation due to major physical stressors, geologic heterogeneity, and nearshore morphology, *Earth-Science Reviews*, 103800.
- Geng, X., and H. A. Michael (2020), Preferential flow enhances pumping - induced saltwater intrusion in volcanic aquifers, *Water Resources Research*, 56(5), e2019WR026390.
- Geng, X., H. A. Michael, M. C. Boufadel, F. J. Molz, F. Gerges, and K. Lee (2020b), Heterogeneity affects intertidal flow topology in coastal beach aquifers, *Geophysical Research Letters*, 47, e2020GL089612.
- Geng, X., Z. Pan, M. C. Boufadel, T. Ozigokmen, K. Lee, and L. Zhao (2016), Simulation of oil bioremediation in a tidally influenced beach: Spatiotemporal evolution of nutrient and dissolved oxygen, *Journal of Geophysical Research: Oceans*, 121(4), 2385-2404.
- Ghasemizadeh, R., F. Hellweger, C. Butscher, I. Padilla, D. Vesper, M. Field, and A. Alshawabkeh (2012), Groundwater flow and transport modeling of karst aquifers, with particular reference to the North Coast Limestone aquifer system of Puerto Rico, *Hydrogeology journal*, 20(8), 1441-1461.
- Gibert, J., D. Danielopol, and J. A. Stanford (1994), *Groundwater ecology*, Academic Press.
- Gingerich, S. B. (2008), Ground-water availability in the Wailuku Area, Maui, Hawai'i *Rep. 2328-0328*,

US Geological Survey.

Gingerich, S. B., and C. I. Voss (2005), Three-dimensional variable-density flow simulation of a coastal aquifer in southern Oahu, Hawaii, USA, *Hydrogeology Journal*, 13(2), 436-450.

Gonnea, M. E., and M. A. Charette (2014), Hydrologic controls on nutrient cycling in an unconfined coastal aquifer, *Environmental science & technology*, 48(24), 14178-14185.

Goswami, R. R., and T. P. Clement (2007), Laboratory - scale investigation of saltwater intrusion dynamics, *Water Resources Research*, 43(4).

Harbaugh, A. W. (2005), *MODFLOW-2005, the US Geological Survey modular ground-water model: the ground-water flow process*, US Department of the Interior, US Geological Survey Reston.

Heiss, J., H. Michael, and M. Koneshloo (2020), Denitrification hotspots in intertidal mixing zones linked to geologic heterogeneity, *Environmental Research Letters*.

Held, R., S. Attinger, and W. Kinzelbach (2005), Homogenization and effective parameters for the Henry problem in heterogeneous formations, *Water resources research*, 41(11).

Helm-Clark, C. M., D. W. Rodgers, and R. P. Smith (2004), Borehole geophysical techniques to define stratigraphy, alteration and aquifers in basalt, *Journal of Applied Geophysics*, 55(1-2), 3-38.

Henry, H. R. (1959), Salt intrusion into fresh - water aquifers, *Journal of Geophysical Research*, 64(11), 1911-1919.

Horn, D. P. (2002), Beach groundwater dynamics, *Geomorphology*, 48(1-3), 121-146.

Horn, D. P. (2006), Measurements and modelling of beach groundwater flow in the swash-zone: a review, *Continental Shelf Research*, 26(5), 622-652.

Houben, G. J., L. Stoeckl, K. E. Mariner, and A. S. Choudhury (2018), The influence of heterogeneity on coastal groundwater flow-physical and numerical modeling of fringing reefs, dykes and structured conductivity fields, *Advances in Water Resources*, 113, 155-166.

Hunt, C., C. Ewart, and C. Voss (1988), Region 27, Hawaiian Islands, *Hydrogeology. The Geological Society of North America, Boulder Colorado. 1988. p 255-262. 5 fig, 13 ref.*

Huyakorn, P., Y. Wu, and N. Park (1996), Multiphase approach to the numerical solution of a sharp interface saltwater intrusion problem, *Water Resources Research*, 32(1), 93-102.

Johannes, R. (1980), The ecological significance of the submarine discharge of groundwater, *Marine Ecology Progress Series*, 365-373.

Kerrou, J., and P. Renard (2010), A numerical analysis of dimensionality and heterogeneity effects on advective dispersive seawater intrusion processes, *Hydrogeology Journal*, 18(1), 55-72.

Kim, K. H., J. W. Heiss, H. A. Michael, W. J. Cai, T. Laattoe, V. E. Post, and W. J. Ullman (2017), Spatial patterns of groundwater biogeochemical reactivity in an intertidal beach aquifer, *Journal of Geophysical Research: Biogeosciences*, 122(10), 2548-2562.

Kim, K. H., H. A. Michael, E. K. Field, and W. J. Ullman (2019a), Hydrologic shifts create complex transient distributions of particulate organic carbon and biogeochemical responses in beach aquifers, *Journal of Geophysical Research: Biogeosciences*, 124(10), 3024-3038.

Kim, K. H., H. A. Michael, E. K. Field, and W. J. Ullman (2019b), Hydrologic shifts create complex transient distributions of particulate organic carbon and biogeochemical responses in beach aquifers, *Journal of Geophysical Research: Biogeosciences*.

Knight, A. C., D. J. Irvine, and A. D. Werner (2021), Alongshore freshwater circulation in offshore aquifers, *Journal of Hydrology*, 593, 125915.

Koneshloo, M., P. Kreyns, and H. A. Michael (2018), Combining process-based and surface-based models to simulate subsurface heterogeneity in volcanic aquifers, *Stochastic Environmental Research*

and Risk Assessment, 1-19.

Kreyns, P., X. Geng, and H. A. Michael (2020), The influence of connected heterogeneity on groundwater flow and salinity distributions in coastal volcanic aquifers, *Journal of Hydrology*, 124863.

Langevin, C. D., D. T. Thorne Jr, A. M. Dausman, M. C. Sukop, and W. Guo (2008), SEAWAT version 4: a computer program for simulation of multi-species solute and heat transport *Rep. 2328-7055*, Geological Survey (US).

Lester, D. R., M. Dentz, and T. L. Borgne (2016), Chaotic mixing in three dimensional porous media, *arXiv preprint arXiv:1602.05270*.

Li, H., M. C. Boufadel, and J. W. Weaver (2008), Tide-induced seawater-groundwater circulation in shallow beach aquifers, *Journal of Hydrology*, 352(1-2), 211-224.

Lu, C., Y. Chen, C. Zhang, and J. Luo (2013), Steady-state freshwater-seawater mixing zone in stratified coastal aquifers, *Journal of hydrology*, 505, 24-34.

Michael, H. A., A. E. Mulligan, and C. F. Harvey (2005), Seasonal oscillations in water exchange between aquifers and the coastal ocean, *Nature*, 436(7054), 1145.

Michael, H. A., K. C. Scott, M. Koneshloo, X. Yu, M. R. Khan, and K. Li (2016), Geologic influence on groundwater salinity drives large seawater circulation through the continental shelf, *Geophysical Research Letters*, 43(20).

Miller, D. C., and W. J. Ullman (2004), Ecological consequences of ground water discharge to Delaware Bay, United States, *Groundwater*, 42(7), 959-970.

Miller, J. A., R. Whitehead, D. S. Oki, S. B. Gingerich, and P. G. Olcott (1997), Ground Water Atlas of the United States: Segment 13, Alaska, Hawaii, Puerto Rico, and the US Virgin Islands *Rep. 0607881267*, US Geological Survey.

Montiel, D., N. Dimova, B. Andreo, J. Prieto, J. García-Orellana, and V. Rodellas (2018), Assessing submarine groundwater discharge (SGD) and nitrate fluxes in highly heterogeneous coastal karst aquifers: Challenges and solutions, *Journal of Hydrology*, 557, 222-242.

Moore, W. S. (1999), The subterranean estuary: a reaction zone of ground water and sea water, *Marine Chemistry*, 65(1-2), 111-125.

Moosdorf, N., M. E. Böttcher, D. Adyasari, E. Erkul, B. S. Gilfedder, J. Greskowiak, A.-K. Jenner, L. Kotwicki, G. Massmann, and M. Müller-Petke (2021), A state-of-the-art perspective on the characterization of subterranean estuaries at the regional scale, *Frontiers in Earth Science*, 9, 95.

Neupauer, R. M., J. D. Meiss, and D. C. Mays (2014), Chaotic advection and reaction during engineered injection and extraction in heterogeneous porous media, *Water Resources Research*, 50(2), 1433-1447.

Nofal, E., M. Amer, S. El-Didy, and A. Fekry (2015), Sea water intrusion in Nile Delta in perspective of new configuration of the aquifer heterogeneity using the recent stratigraphy data, *J Am Sci*, 11(6), 281-292.

Oki, D., S. Gingerich, and R. Whitehead (1999), Hawaii In Ground Water Atlas of the United States, Segment 13, Alaska, Hawaii, Puerto Rico, and the US Virgin Islands: US Geological Survey Hydrologic Investigations Atlas 730-N, p, N12 N, 22, N36.

Rathore, S. S., Y. Zhao, C. Lu, and J. Luo (2018), Defining the effect of stratification in coastal aquifers using a new parameter, *Water Resources Research*, 54(9), 5948-5957.

Remy, N., A. Boucher, and J. Wu (2009), *Applied geostatistics with SGeMS: A user's guide*, Cambridge University Press.

Robinson, C., B. Gibbes, H. Carey, and L. Li (2007), Salt - freshwater dynamics in a subterranean estuary over a spring - neap tidal cycle, *Journal of Geophysical Research: Oceans*, 112(C9), C09007.

- Robinson, C. E., P. Xin, I. R. Santos, M. A. Charette, L. Li, and D. A. Barry (2018), Groundwater dynamics in subterranean estuaries of coastal unconfined aquifers: Controls on submarine groundwater discharge and chemical inputs to the ocean, *Advances in Water Resources*, *115*, 315-331.
- Rowland, S. K., and G. P. Walker (1990), Pahoehoe and aa in Hawaii: volumetric flow rate controls the lava structure, *Bulletin of Volcanology*, *52*(8), 615-628.
- Santos, I. R., B. D. Eyre, and M. Huettel (2012), The driving forces of porewater and groundwater flow in permeable coastal sediments: A review, *Estuarine, Coastal and Shelf Science*, *98*, 1-15.
- Santos, I. R. S., W. C. Burnett, J. Chanton, B. Mwashote, I. G. Suryaputra, and T. Dittmar (2008), Nutrient biogeochemistry in a Gulf of Mexico subterranean estuary and groundwater - derived fluxes to the coastal ocean, *Limnology and Oceanography*, *53*(2), 705-718.
- Sawyer, A. H., O. Lazareva, K. D. Kroeger, K. Crespo, C. S. Chan, T. Stieglitz, and H. A. Michael (2014), Stratigraphic controls on fluid and solute fluxes across the sediment—water interface of an estuary, *Limnology and Oceanography*, *59*(3), 997-1010.
- Sebben, M. L., and A. D. Werner (2016), A modelling investigation of solute transport in permeable porous media containing a discrete preferential flow feature, *Advances in water resources*, *94*, 307-317.
- Sebben, M. L., A. D. Werner, and T. Graf (2015), Seawater intrusion in fractured coastal aquifers: A preliminary numerical investigation using a fractured Henry problem, *Advances in water resources*, *85*, 93-108.
- Siena, M., and M. Riva (2018), Groundwater withdrawal in randomly heterogeneous coastal aquifers, *Hydrology and Earth System Sciences*, *22*(5), 2971-2985.
- Simmons, C. T., T. R. Fenstemaker, and J. M. Sharp Jr (2001), Variable-density groundwater flow and solute transport in heterogeneous porous media: approaches, resolutions and future challenges, *Journal of Contaminant Hydrology*, *52*(1-4), 245-275.
- Simmons Jr, G. M. (1992), Importance of submarine groundwater discharge (SGWD) and seawater cycling to material flux across sediment/water interfaces in marine environments, *Marine Ecology Progress Series*, 173-184.
- Slomp, C. P., and P. Van Cappellen (2004), Nutrient inputs to the coastal ocean through submarine groundwater discharge: controls and potential impact, *Journal of Hydrology*, *295*(1-4), 64-86.
- Taniguchi, M., H. Dulai, K. M. Burnett, I. R. Santos, R. Sugimoto, T. Stieglitz, G. Kim, N. Moosdorf, and W. C. Burnett (2019), Submarine groundwater discharge: updates on its measurement techniques, geophysical drivers, magnitudes, and effects, *Frontiers in Environmental Science*, *7*, 141.
- Wentworth, C. K., and G. A. Macdonald (1953), Structures and forms of basaltic rocks in Hawaii *Rep.*, US Govt. Print. Off.
- Xin, P., C. Robinson, L. Li, D. A. Barry, and R. Bakhtyar (2010), Effects of wave forcing on a subterranean estuary, *Water Resources Research*, *46*(12).
- Xu, Z., S. W. Bassett, B. Hu, and S. B. Dyer (2016), Long distance seawater intrusion through a karst conduit network in the Woodville Karst Plain, Florida, *Scientific Reports*, *6*, 32235.
- Xu, Z., B. X. Hu, and M. Ye (2018), Numerical modeling and sensitivity analysis of seawater intrusion in a dual-permeability coastal karst aquifer with conduit networks, *Hydrology and Earth System Sciences*, *22*(1), 221.
- Yang, J., T. Graf, and T. Ptak (2015), Sea level rise and storm surge effects in a coastal heterogeneous aquifer: a 2D modelling study in northern Germany, *Grundwasser*, *20*(1), 39-51.
- Zhou, Y., C. Kellermann, and C. Griebler (2012), Spatio-temporal patterns of microbial communities in a hydrologically dynamic pristine aquifer, *FEMS microbiology ecology*, *81*(1), 230-242.

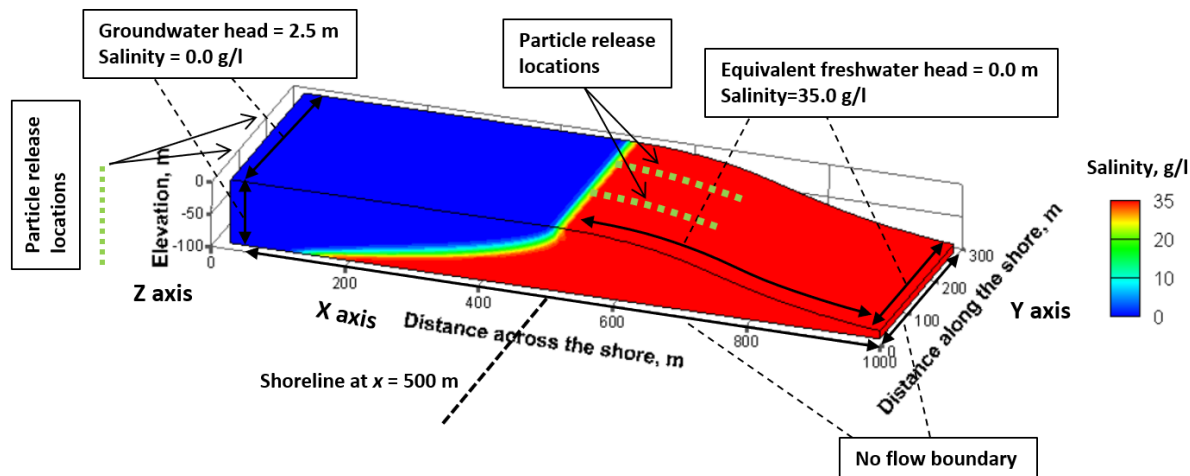


Figure 1 Model setup. Boundary conditions implemented in the three-dimensional simulations of groundwater flow and salt transport using SEAWAT v4.0. The simulations were run to steady state for hydraulic heads and concentrations. The neutrally buoyant particles were released at two alongshore locations ($Y = 14$ and 20 m) and at two across-shore locations (onshore and offshore). The onshore particles were released at 10 m depth interval along the vertical inland boundary, spanning from $Z = 0$ to -100 m. The offshore particles were released along the sea floor boundary from $X = 550$ m to 700 m.

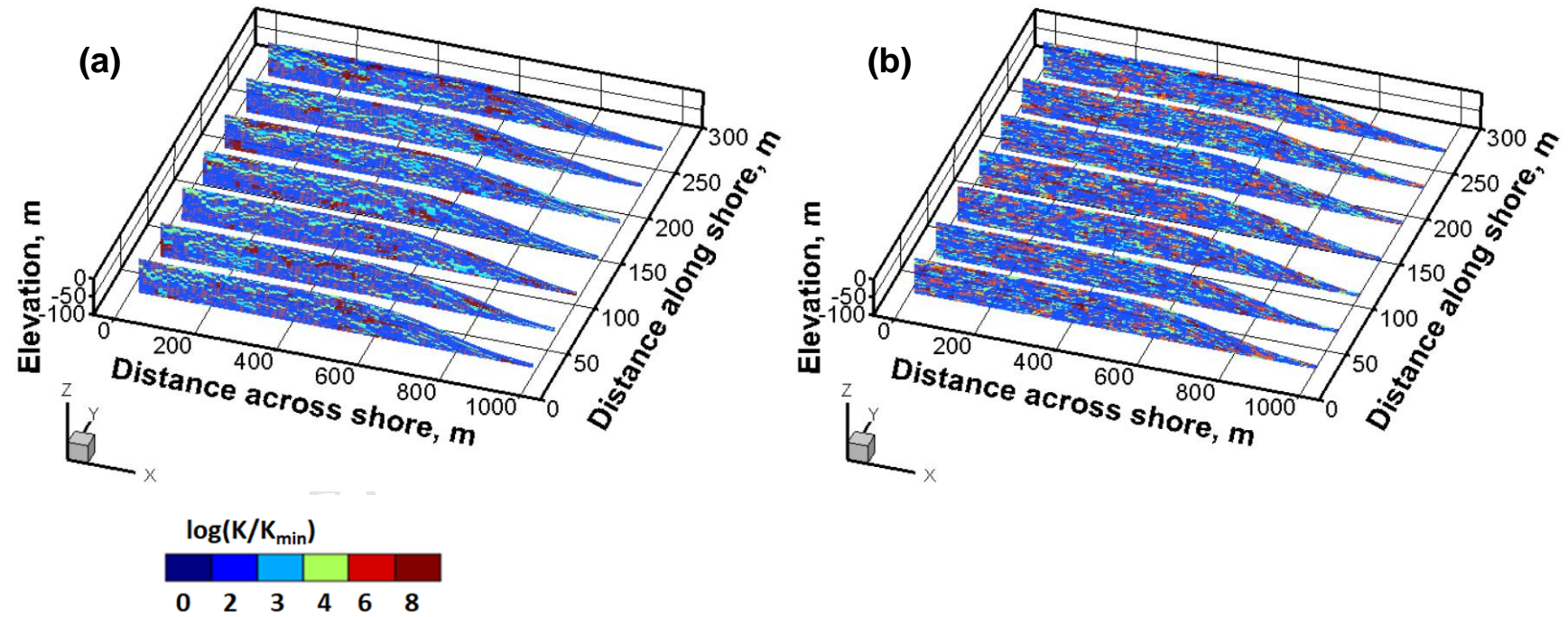


Figure 2 Example of heterogeneous K fields for (a) conduit and (b) SIS cases, respectively. The $\log(K/K_{\min})$ values of 0, 2, 3, 4, 6, 8 denote the heterogeneous facies of ash, aa, transitional lava, pahoehoe, clinker and lava tube, respectively.

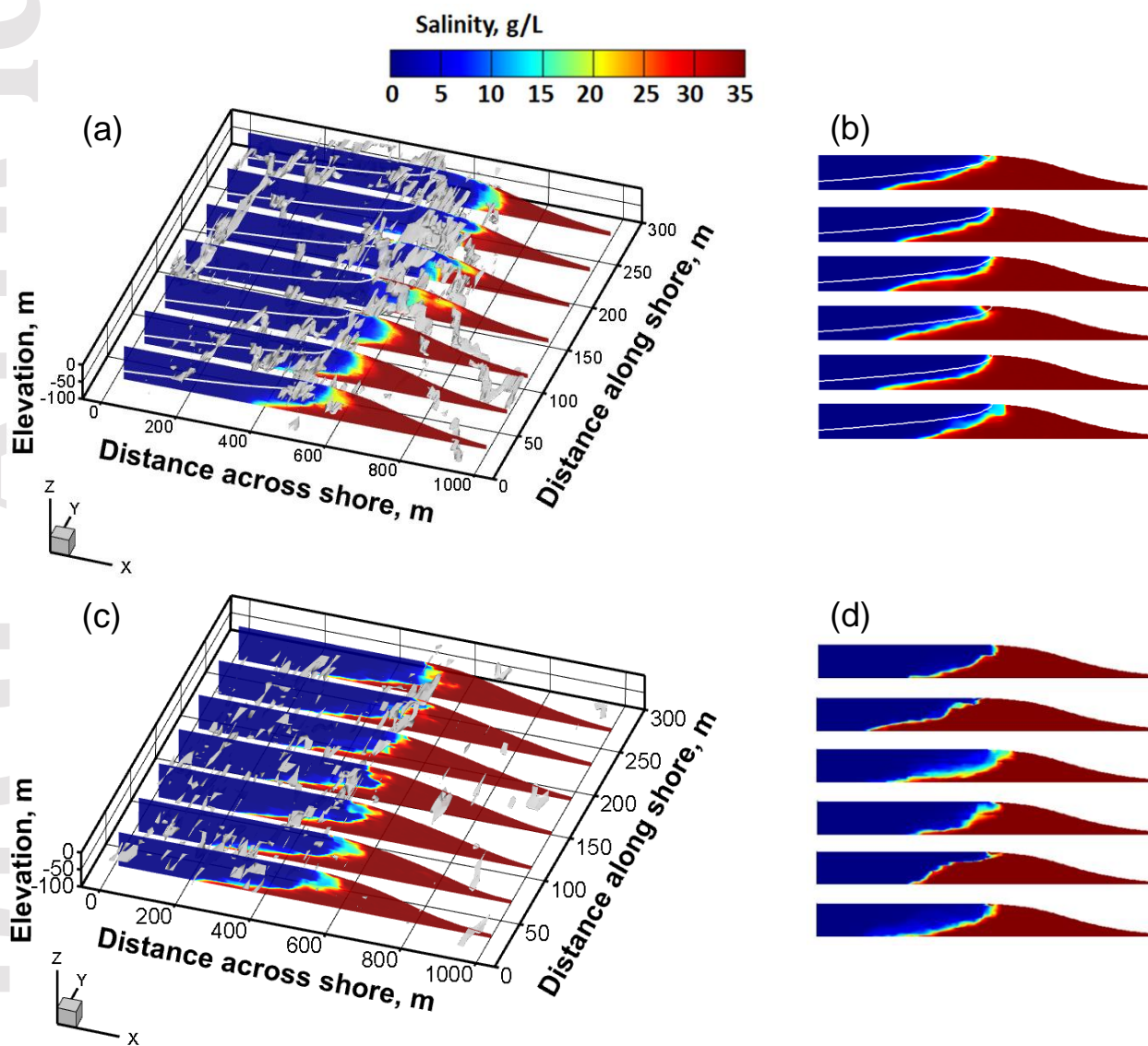


Figure 3 Example of simulated 3D (a, c) and 2D (b, d) steady-state salinity distributions for (a, b) conduit and (c, d) SIS cases, respectively. White lines in a and b show locations of transition zone for corresponding equivalent homogeneous cases. Gray conduits in a and c show preferential flow zones with velocity 8 orders of magnitude higher than minimum velocity simulated in each heterogeneous field.

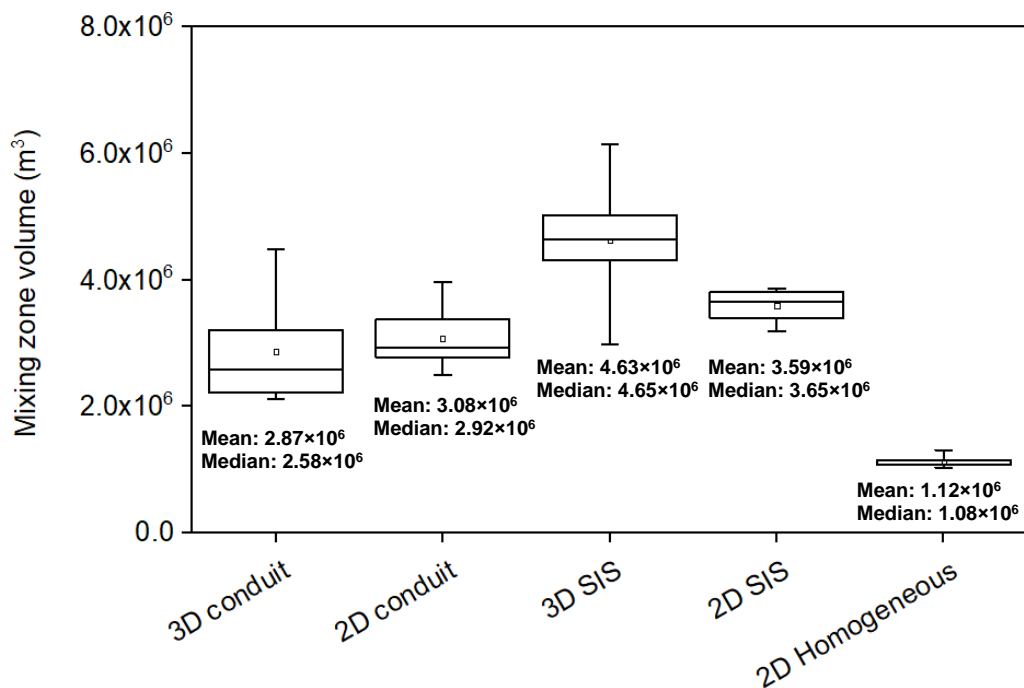


Figure 4 Comparison of mixing zone volume for the simulated cases. Note that 2D and 3D Homogeneous cases are identical. Top and bottom of the rectangles represent the 25th and 75th percentiles of the data set. Solid line and cube indicate median and mean values, respectively. Whiskers indicate maximum and minimum values. Six geologic realizations were considered for conduit, equivalent homogeneous, and SIS cases.

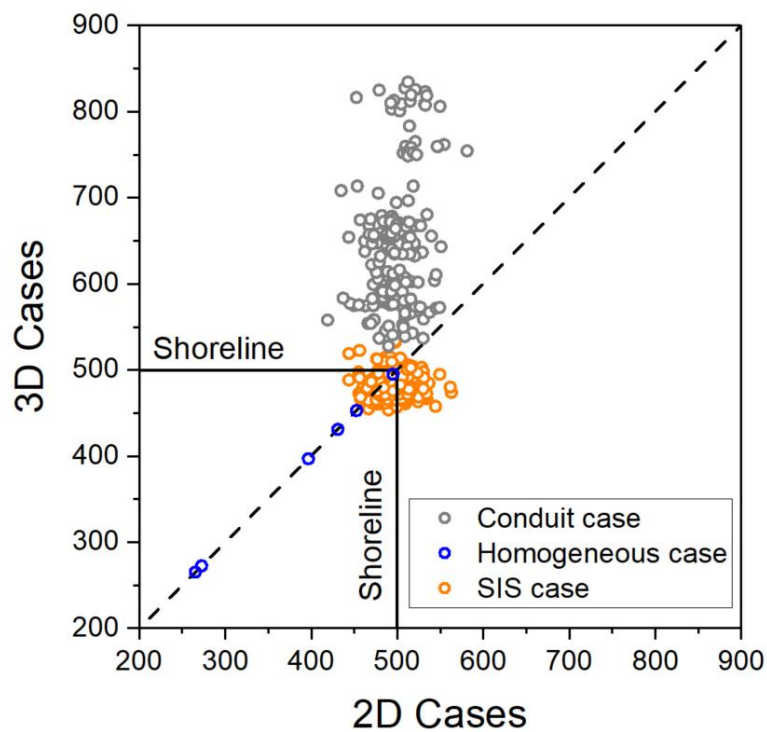


Figure 5 Comparison of mixing zone centroid between 3D and 2D simulations for conduit, equivalent homogeneous, and SIS cases. The distance (in meter) shown in horizontal and vertical axes represents the mixing zone centroid of across-shore slices simulated by 2D and 3D models, respectively, for conduit, equivalent homogeneous, and SIS cases.

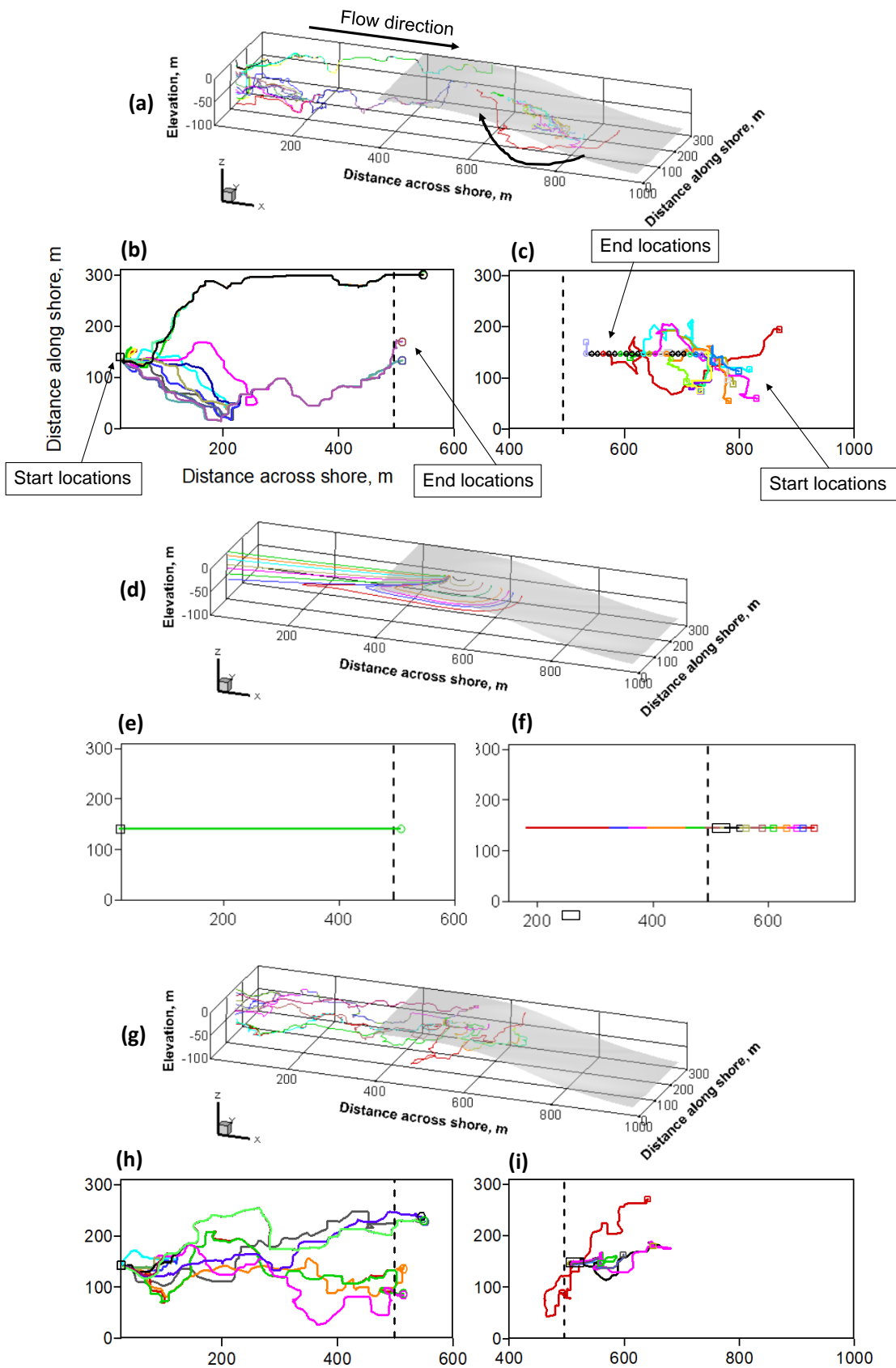


Figure 6 Examples of 3D trajectory of particles released from inland (left, top view) and offshore (right, top view) for (a-c) conduit, (d-f) equivalent homogeneous, and (g-i) SIS cases, respectively. Top view of the trajectories is to highlight lateral movement of particle flowpaths. Different particle trajectories are marked with different colors. The start and end locations of particle flow paths are marked with square and circle symbols, respectively; dashed line denotes shoreline location. Backward particle tracking scheme was implemented to trace trajectory of offshore particles, and thus particles released at recharge locations could not be traced. These recharge locations are marked in black for conduit cases; for equivalent homogeneous and SIS cases, offshore particles released within the groundwater discharge zone only occurred between $X = 500$ m and 550 m, and were marked with a black outline.

Accepted Article

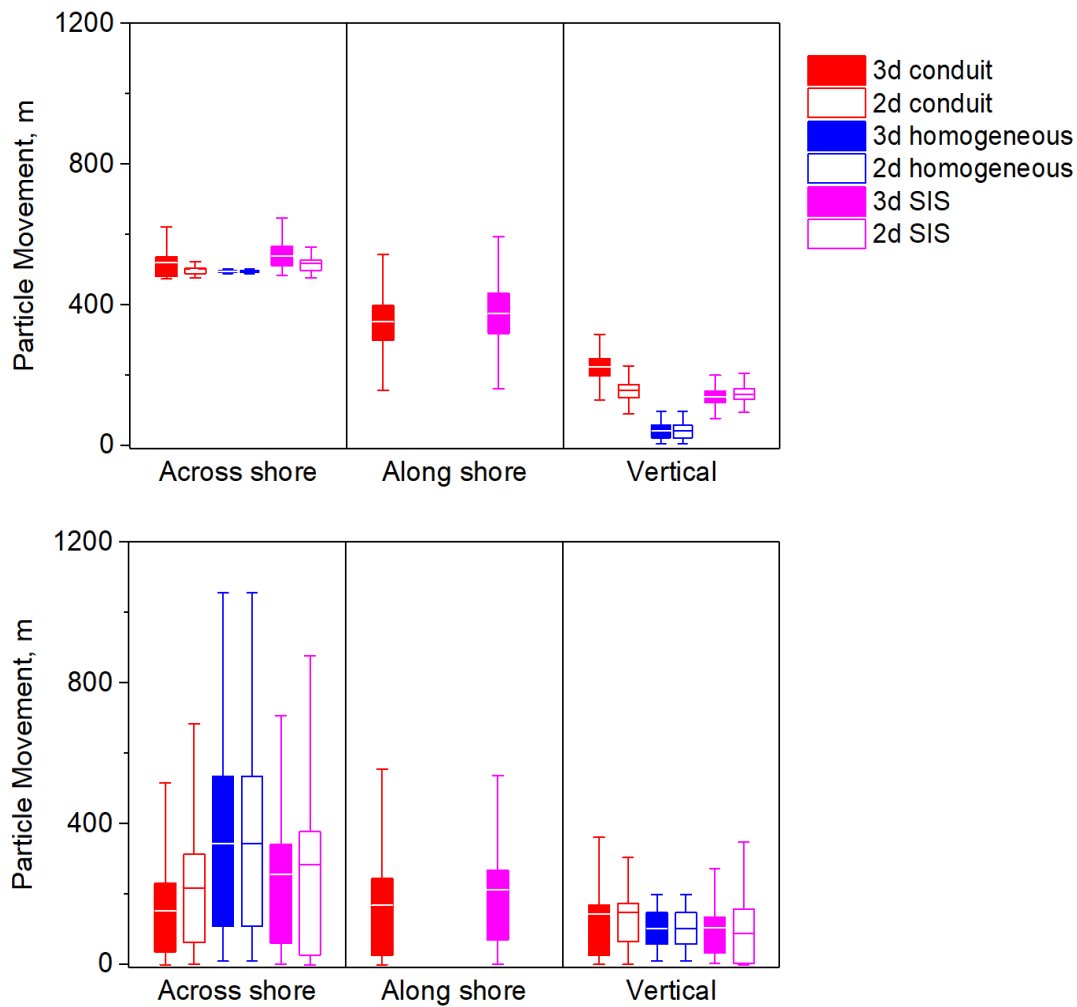


Figure 7 Travel distance in across-shore, along-shore, and vertical directions for particles released from (a) inland and (b) the seawater-groundwater recirculation zone, respectively, for all heterogeneous realizations. The lateral movement of groundwater (i.e., alongshore movement) was zero by definition in 2D cases. Bar, box, and line display the full range of variation (from min to max), the likely range of variation (i.e., from 25th percentile to 75th percentile), and the mean value, respectively.

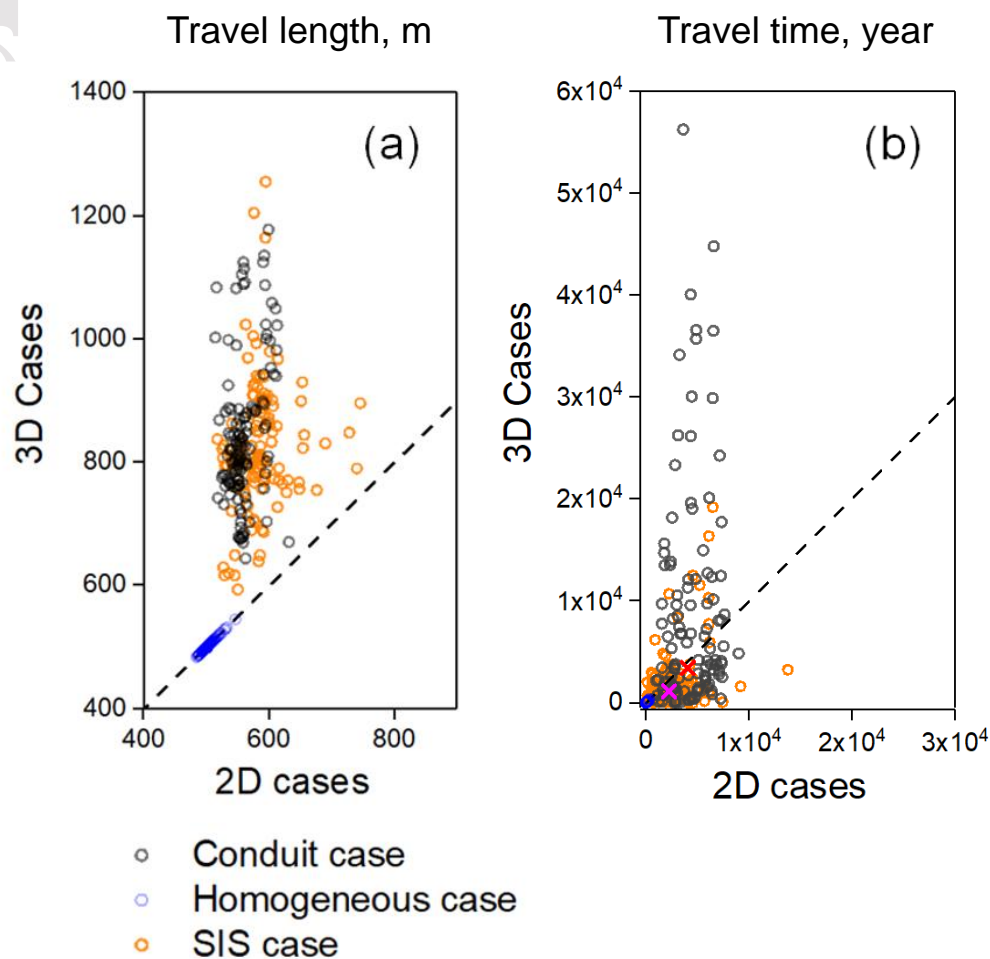


Figure 8 Comparison of (a) travel length and (b) travel time of particles released from inland between 2D and 3D conduit, equivalent homogeneous, and SIS cases. The particle travel length is calculated based on Eq. (1). The cross symbols marked with red and purple color represent the median travel time for conduit and SIS cases, respectively.

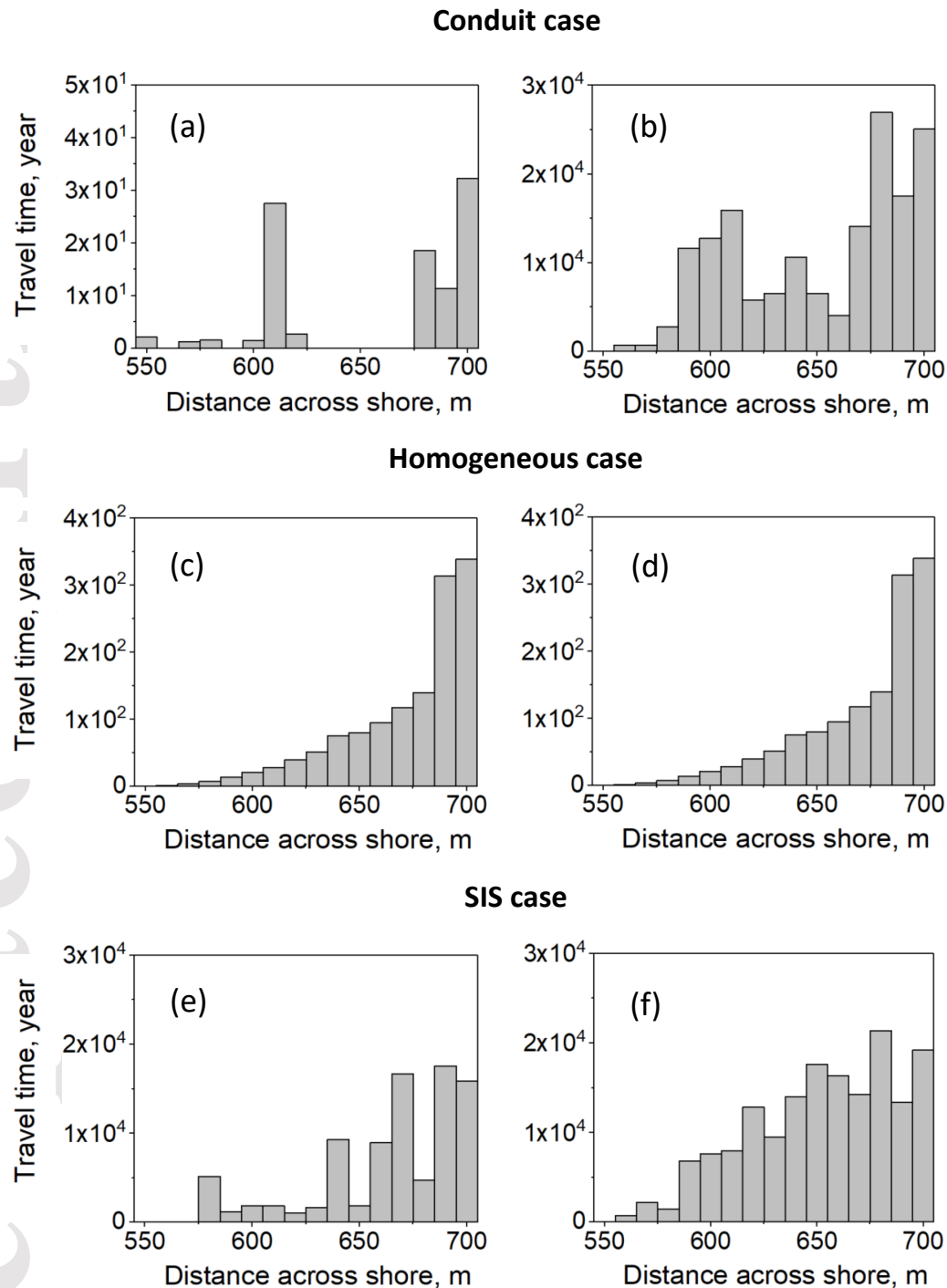


Figure 9 Examples of spatial distribution of travel time for particles released offshore, from the seawater-groundwater recirculation zone for (a) 3D conduit case, (b) 2D conduit case, (c) 3D homogeneous case, (d) 2D homogeneous case, (e) 3D SIS case, and (f) 2D SIS case. The particles were released in offshore recharge locations from $x = 550$ m to 700 m along $Y = 140$ m. Forward particle tracking was implemented to quantify travel time of particles released along the offshore major recharge zone with 10 m intervals.

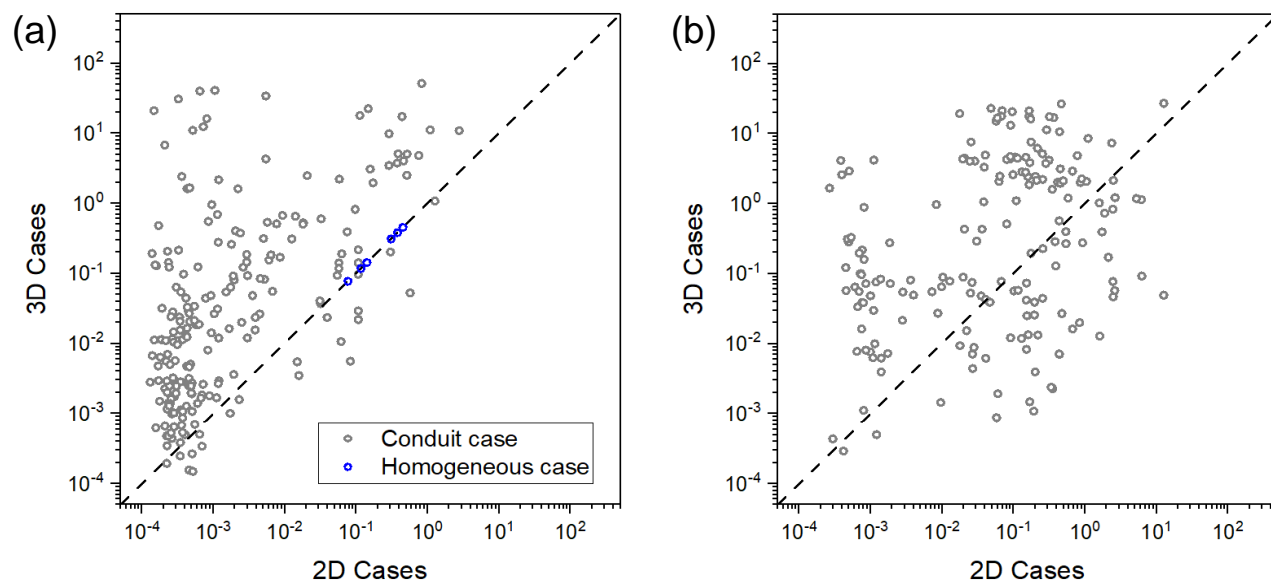


Figure 10 Comparison of saline SGD (m/d) between 2D and 3D simulations for (a) conduit and equivalent homogeneous and (b) SIS cases.